High spectral resolution lidar to measure optical scattering properties of atmospheric aerosols. 2: Calibration and data analysis

J. T. Sroga, E. W. Eloranta, S. T. Shipley, F. L. Roesler, and P. J. Tryon

The high spectral resolution lidar (HSRL) measures optical properties of atmospheric aerosols by interferometrically separating the elastic aerosol backscatter from the Doppler broadened molecular contribution. Calibration and data analysis procedures developed for the HSRL are described. Data obtained during flight evaluation testing of the HSRL system are presented with estimates of uncertainties due to instrument calibration. HSRL measurements of the aerosol scattering cross section are compared with *in situ* integrating nephelometer measurements.

I. Introduction

This paper describes the calibration and data analysis procedures necessary to measure the optical scattering properties of atmospheric aerosols using a high spectral resolution lidar (HSRL). As discussed in the companion paper,[1] the HSRL technique measures optical properties of atmospheric aerosols by separating the elastic backscattered aerosol signal from the thermal Doppler broadened molecular backscattered contribution. The aerosol–molecular separation is achieved using a high spectral resolution Fabry-Perot optical interferometer. Lidar backscatter contributions near the laser wavelength (primarily aerosol contributions) are transmitted through the interferometer filter to an aerosol channel detector. Light not transmitted through the filter is reflected to a molecular channel detector which measures those photons which have been Doppler shifted.

The spectral transmission functions of the receiver spectrometer are modeled to determine the relative contributions of aerosol and molecular backscatter in each channel. A least-squares technique is used to estimate the spectrometer model parameters from measurements of the receiver spectral distribution obtained with diffuse uniform laser illumination of the spectrometer entrance aperture. The HSRL calibration is a function of the scattering volume distance due to variations in the angular distribution of backscattered light incident upon the spectrometer entrance aperture. A ray tracing technique is used in conjunction with the theoretical spectrometer model to compute the range dependence of the instrumental calibration.

Preliminary analysis of HSRL data obtained during flight evaluation testing is also presented to demonstrate the feasibility of the HSRL technique. These data were acquired during daylight conditions with a 2-mW average laser output power. The HSRL-derived scattering properties are compared to *in situ* measurements obtained by an integrating nephelometer installed in an instrumented light aircraft. This intercomparison illustrates the capabilities of the HSRL to remotely measure aerosol optical scattering properties. A sensitivity analysis of the measured optical properties to uncertainties in the HSRL calibration has shown which procedures are most critical.

II. Calibration Theory

The HSRL system measures aerosol optical scattering properties by using the backscatter from the molecular atmosphere as a known target. The receiver spectrometer separates the atmospheric backscatter intensity into two channels, each a linear combination of aerosol and molecular contributions. The signals measured in each channel are given by (Shipley *et al.*[1])

$$S_a(R) = \gamma[C_{aa}(R) \cdot N_a(R) + C_{ma}(R) \cdot N_m(R)] + B_a, \quad (1a)$$

When this work was initiated, all authors were with University of Wisconsin, Madison, Wisconsin 53706, J. T. Sroga, E. W. Eloranta and S. T. Shipley in the Meteorology Department, F. L. Roesler and P. J. Tryon in the Physics Department. At present, J. T. Sroga is with RCA Astro-Electronics, Princeton, New Jersey 08540; S. T. Shipley is with NASA Langley Research Center, Hampton, Virginia 23665; and P. J. Tryon is with Gilson Medical Electronics, Madison, Wisconsin 53717.

Received 12 September 1983.
0003-6935/83/233725-08$01.00/0.

$$S_m(R) = \gamma[C_{am}(R) \cdot N_a(R) + C_{mm}(R) \cdot N_m(R)] + B_m, \quad (1b)$$

where R signal range,
$S_a(R), S_m(R)$ signal levels measured in the aerosol and molecular channels, respectively,
$N_a(R), N_m(R)$ total number of aerosol and molecular backscattered photons,
B_a, B_m background signal intensities in the aerosol and molecular channels,
$C_{aa}(R), C_{ma}(R)$ fraction of total aerosol and molecular backscatter detected in the aerosol channel,
$C_{am}(R), C_{mm}(R)$ fraction of total aerosol and molecular backscatter detected in the molecular channel, and
γ constant which includes conversion efficiency of the HSRL system. The efficiency performance of the HSRL system is described by Sroga.[2]

Equations (1a) and (1b) can be inverted to measure the pure aerosol and molecular backscatter once the calibration coefficients C_{aa}, C_{am}, C_{ma}, and C_{mm} are determined.

The calibration coefficients are determined from the spectral distributions of the laser transmitter, receiver spectrometer bandpass, and the light backscattered from aerosols and molecules. Since the Doppler broadened aerosol backscatter spectral distribution for a monochromatic source is 1–2 orders of magnitude smaller than the transmitter bandwidth, we have assumed in this analysis that the aerosol backscatter spectral distribution is essentially the same as the laser spectral distribution. The fraction of the total aerosol contribution in each channel is given by the convolution of the laser spectral distribution $\mathcal{L}(\sigma - \sigma_0)$, with the receiver spectral transmission in each channel, $T_a(R,\sigma - \sigma_r)$ and $T_m(R,\sigma - \sigma_r)$, so that

$$C_{aj}(R,\sigma^*) = \int_{-\infty}^{\infty} \mathcal{L}(\sigma - \sigma_0) \cdot T_j(R,\sigma - \sigma_r) d\sigma \quad j = a,m, \quad (2)$$

where σ_0 wave number of the peak laser intensity,
σ_r wave number of the aerosol channel peak transmission, and
$\sigma^* = \sigma_0 - \sigma_r$ laser-spectrometer relative detuning wave number.

The molecular contribution in each channel is given by the convolution of Eq. (2) with the molecular backscatter spectral distribution

$$C_{mj}(R,\sigma^*) = \int_{-\infty}^{\infty} \frac{1}{N_m} \frac{dN_m(\sigma' - \sigma_0)}{d\sigma'} \int_{-\infty}^{\infty} (\sigma - \sigma_0) \cdot T_j(\sigma - \sigma' - \sigma_r) d\sigma d\sigma' \quad j = a,m. \quad (3)$$

Under atmospheric conditions, the molecular backscattered spectrum exhibits a nearly Gaussian line shape due to Doppler broadening. The Gaussian line shape for an ideal gas of mean molecular mass $\overline{m}$ at an equilibrium temperature T is given by[3]

$$\frac{1}{N_m} \frac{dN_m}{d\sigma} = \sqrt{\frac{\overline{m}c^2}{8\pi\sigma_0^2 kT}} \exp\left[\frac{-\overline{m}c^2}{8\sigma_0^2 kT}(\sigma - \sigma_0)^2\right], \quad (4)$$

where c is the speed of light and k is Boltzmann's constant. Deviations from the Gaussian molecular backscattered spectral distributions can occur due to scattering from correlated pressure fluctuations in the atmosphere.[4] The sensitivity of Eq. (3) to the shape of the molecular backscattered spectrum was investigated using the kinetic model of Yip and Nelkin.[5] The molecular coefficients C_{ma}, C_{mm} computed from Eq. (4) are in error by <1.5% from those computed using the kinetic model. This error is the same magnitude as a temperature uncertainty of ±10 K in Eq. (4). We conclude that the HSRL technique is relatively insensitive to the shape of the molecular spectrum over the range of conditions in the atmosphere.

The spectrometer used to achieve this aerosol and molecular backscatter separation is described in more detail in the companion paper.[1] The spectral distribution of each channel is the product of the transmission through the three-etalon prefilter $[T_p(R,\sigma^*)]$ and the high resolution etalon transmission and reflection response functions $[T_{HR}(R,\sigma^*), R_{HR}(R,\sigma^*)]$, respectively:

$$T_a(R,\sigma^*) = A_a \cdot T_p(R,\sigma^*) \cdot T_{HR}(R,\sigma^*); \quad (5a)$$

$$T_m(R,\sigma^*) = A_m \cdot T_p(R,\sigma^*) \cdot R_{HR}(R,\sigma^*). \quad (5b)$$

Amplitude factors A_a and A_m account for light losses in each channel at mirror and lens surfaces. The transmission function of a Fabry-Perot interferometer can be modeled using the interferometer design parameters and the angular distribution of light incident upon the etalon. The theoretical spectral transmission distribution of the three-etalon prefilter is given by[6]

$$T_p(R,\sigma^*) = \iint_{\text{aperture}} I_a(x,y,R) \cdot \left[\prod_{i=1}^{3} a_i(\sigma^*,x,y)\right] dxdy, \quad (6)$$

where $I_a(x,y,R)$ is the backscattered intensity distribution in the entrance aperture produced by light scattered from a range R, and a_i is the Airy function for the ith etalon

$$a_i(\sigma^*) = \left(\frac{1 - \rho_i - \alpha_i}{1 - \rho_i}\right)^2 \cdot \left[1 + \frac{4N_i^2}{\pi^2} \cdot \sin^2(2\pi n_i l_i(\sigma^* - \sigma_i)\cos\theta_i\right]^{-1}, \quad (7)$$

where N_i prefilter ith etalon reflectivity finesse,
n_i index of refraction of the ith etalon chamber,
l_i ith etalon spacer length,
σ_i wave number of ith etalon peak transmission,
ρ_i ith etalon reflectivity,
α_i ith etalon absorptivity, and
θ_i angle of the incident light with respect to the etalon axis.

The incidence angle θ can be calculated from the formula

$$\cos\theta = \frac{\mathbf{r} \cdot \mathbf{r}_I + f^2}{[(r^2 + f^2)(r_I^2 + f^2)]^{1/2}}, \quad (8)$$

where $\mathbf{r}$ is the radius vector in the aperture plane from

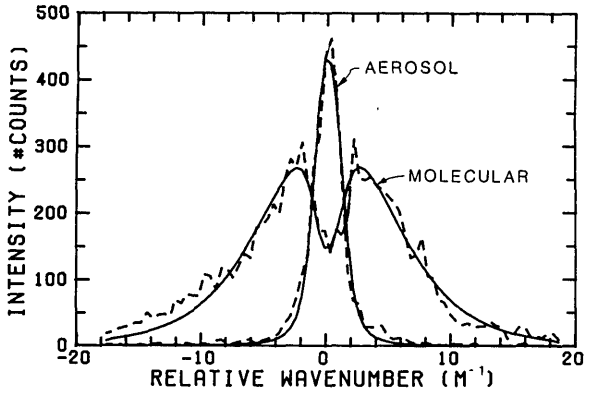

Fig. 1. Measurements of the aerosol and molecular channel bandpass distributions convoluted with the laser spectrum, as measured during the 24 July 1980 evaluation flight. The dashed curves are measurements obtained with diffuse uniform laser illumination of the spectrometer entrance aperture. The solid curves are the least-squares estimates of the model calculations [Eqs. (10a),(10b)].

the origin to a point in the aperture (x,y), $\mathbf{r}_I$ is the radius vector from the origin to the intercept of the etalon axis with the aperture plane, and f is the focal length of the collimating lens. The high resolution etalon response functions are given by

$$T_{HR}(R,\sigma^*) = \iint_{\text{aperture}} I'_a(x',y',R)\cdot a_4(\sigma^*,x',y')dx'dy', \quad (9a)$$

$$R_{HR}(R,\sigma^*) = (1-\alpha_{HR}) \iint_{\text{aperture}} I'_a(x',y',R) \cdot [1 - g\cdot a_4(\sigma^*,x',y')]^2 dx'dy', \quad (9b)$$

where

$$g = 1 - \frac{\alpha_4^2\rho_4}{(1-\alpha_4)(1-\rho_4)^2}.$$

The aperture intensity distribution I'_a is written in terms of reduced coordinate variables ($x' = 0.6x, y' = 0.6y$) to account for an angular reduction of the entrance aperture image produced by intervening lenses.

The range dependence of the aperture intensity distribution is calculated using a simple ray tracing model of the HSRL transmitter–receiver telescope geometry. This model computes the fraction of the total received backscattered illumination which is transmitted through an area $dxdy$ as a function of position in the entrance aperture. A more detailed description of the ray tracing model is described in the Appendix. Receiver–transmitter geometry parameters listed in Tables I and II of the companion paper[1] are used in these calculations.

III. Experimental Calibration Results

The spectral bandpass of each channel is dependent on the optical alignment of the spectrometer, etalon plate flatness and defects, spectral alignment of the individual interferometric elements, and light losses at mirror and lens surfaces. The bandpass of each channel is experimentally measured by spectrally scanning the receiver spectrometer past the fixed wavelength laser output. Diffuse and attenuated laser light is used to illuminate uniformly the spectrometer entrance aperture during the spectral scan, and the transmission signals are obtained from integration of the photomultiplier afterpulsing detected by the pulse counting electronics. The afterpulse signals are integrated from 2 to 10 μsec after the laser pulse and normalized to account for differences between phototube afterpulsing in each channel.[1] This procedure allows direct measurement of the transmission detection efficiency for both the optical and electronic subsystems, while eliminating electronic noise in the pulse counting system first data bin caused by the laser. Figure 1 illustrates the relative spectral distribution for each channel from data obtained on 24 July 1980.

The measurements shown in Fig. 1 are modeled using the theoretical calculations of the spectrometer spectral distributions [Eqs. (5a) and (5b)] convoluted with the spectral distribution of the laser. The laser spectral distribution is modeled as the square of the Airy function of the dye laser stripping etalon to account for the double-pass arrangement.[1] The model equations for the dual-channel spectrometer are

$$\tilde{T}_a(u,\sigma^*) = \int_{-\infty}^{\infty} T_a(u,\sigma' - \sigma^*)\cdot \mathcal{L}(\sigma')d\sigma', \quad (10a)$$

$$\tilde{T}_m(u,\sigma^*) = \int_{-\infty}^{\infty} T_m(u,\sigma' - \sigma^*)\cdot \mathcal{L}(\sigma')d\sigma', \quad (10b)$$

where u corresponds to a uniform aperture illumination. A least-squares estimate[7] of Eqs. (10a) and (10b) using a uniform aperture intensity is also shown in Fig. 1. The following model parameters were chosen as variables in the regression:

- A_a, A_m aerosol and molecular amplitude factors to account for transmission losses at mirror and lens interfaces.
- N_4 high resolution etalon reflectivity finesse. This parameter allows for adjustment of the width of the high resolution transmission band.
- N_p premonochromator etalon finesse. This parameter allows for adjustment of the prefilter bandwidth ($N_p = N_1 = N_2 = N_3$).
- $\sigma_r - \sigma_p$ relative wave number displacement of prefilter peak transmission from that of the high resolution etalon ($\sigma_1 = \sigma_2 = \sigma_3 = \sigma_p$).
- N_L reflectivity finesse of the laser etalon.

Once the above parameters have been determined for a uniform aperture illumination, the range dependence of the calibration coefficients can be calculated from Eqs. (2) and (3) using the range dependent aperture intensity distribution computed by the method outlined in the Appendix. The variation in the backscattered intensity distribution in the spectrometer aperture slightly decreases the width of the spectrometer passbands and displaces the peak transmission wave number with range. Figure 2 illustrates the range dependence of the calibration coefficients for the 24 July 1980 calibration data. These calculations include corrections to the lidar equation for signal compression due to incomplete geometrical beam overlap. The variations in the calibration coefficients with range are largest inside 2.5 km.

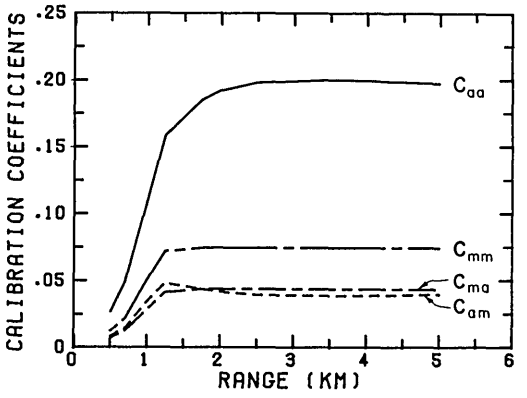

Fig. 2. Range dependence of the HSRL calibration coefficients computed from Eqs. (2) and (3). The spectrometer model parameters were obtained from the least-squares regression estimate shown in Fig. 1 and the range dependence of the aperture intensity distribution described in the Appendix. These coefficients include signal reduction at close ranges (<1.5 km) due to incomplete transmitter–receiver overlap. The variations in the calibration coefficients are largest at ranges close to the receiver telescope.

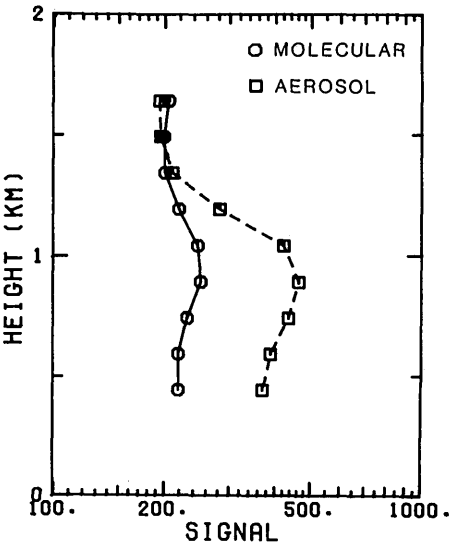

Fig. 3. Signals S_aR^2,S_mR^2 measured by the dual-channel HSRL spectrometer from 1203 to 1220 EDT on 24 July 1980. Aircraft altitude was ~3.2 km ASL. These signals have had background photon counting rates and afterpulsing effects removed before being corrected for the range squared attenuation. The aerosol cross talk in the molecular channel is clearly evident in the mixed layer.

IV. Data Analysis

An evaluation flight experiment was conducted on 24 July 1980 with the HSRL operated in a nadir or down looking mode from the NASA/Wallops Electra. This experiment was designed to compare the HSRL measurements of the spatial distribution of aerosol scattering properties with ground truth measurements. *In situ* measurements of temperature, dew point, and integrating nephelometer measurements of the aerosol scattering cross section were obtained from an instrumented light aircraft[8] for this intercomparison. Data along a short segment of the electra flight path (40°15′N, 81°45′W–39°50′N, 83°00′W, 1203–1220 EDT) were chosen for analysis corresponding to approximately the same time as the *in situ* aircraft measurements (38°10′N, 82°55′W, 1200–1226 EDT). Operation of the HSRL system included alignment of the receiver and transmitter optics and adjustment of the Fabry-Perot interferometric elements while airborne. The spectral alignment of these interferometric elements[1] was also completed while in flight.

The accumulated HSRL signals for both the aerosol and molecular channels are shown in Fig. 3. Individual profiles (~5-sec averages) which showed backscatter contributions from clouds were selectively removed from the data before analysis. These signals have had the background photon counting rate and photomultiplier afterpulsing removed before being corrected for the range squared attenuation. The statistical fluctuations in the signal levels were further reduced by filtering and averaging the data over 150-m intervals. The measurements in the aerosol channel show a relatively clear atmosphere above an aerosol laden mixed layer. The aerosol scattering cross talk in the molecular channel is also clearly seen in this figure. Removal of this cross talk in the molecular channel depends critically upon the instrumental calibration.

The instrumental calibration (see Sec. III of this paper) was determined from measurements of the spectral transmission of each channel (Fig. 1) made prior to the start of the data segment. During the data segment, diffuse laser light was periodically inserted to illuminate uniformly the spectrometer entrance aperture. These signal levels yield a direct measurement of the ratio of the aerosol coefficients C_{aa}/C_{am} for uniform aperture illumination, allowing one to determine the relative spectral alignment of the spectrometer transmission peak with respect to the laser wavelength. The range dependent calibration coefficients (Fig. 2) were calculated at this relative spectral position using the models of the receiver spectrometer response and receiver–transmitter geometry. Parameters of the receiver–transmitter geometry model were adjusted slightly to approximately reproduce the geometrical signal overlap observed in the data and the ratio of the aerosol coefficients C_{aa}/C_{am} obtained from the reflections off the ground surface.

Error analysis of the HSRL measured optical scattering properties is based on the uncertainty in the instrumental calibration. The calibration uncertainties are estimated from statistical fluctuations in the relative spectral tuning of the receiver spectrometer with the laser transmitter, the geometrical alignment of the receiver transmitter optics, and the estimates of the spectrometer model parameters. Diffuse light from the dye laser output was periodically used to uniformly illuminate the spectrometer entrance aperture to measure the relative transmission in each channel during the data acquisition period. The uncertainty in the receiver–transmitter spectral alignment was estimated from the standard deviation in the ratio of these measurements. Uncertainties in the spectrometer model

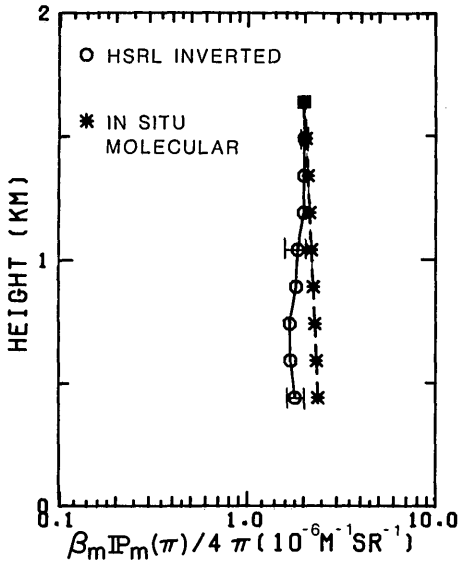

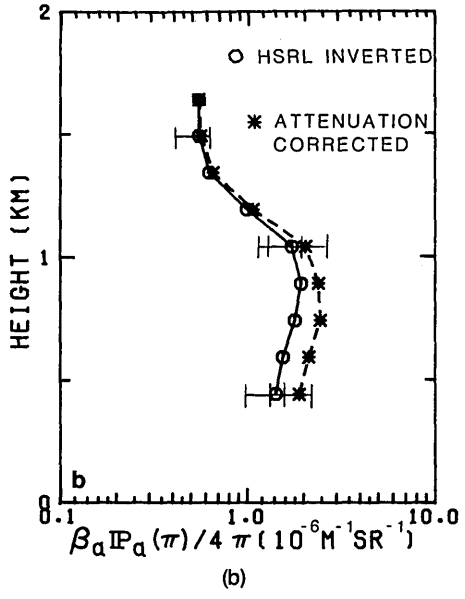

Fig. 4. Molecular and aerosol backscatter cross sections without attenuation corrections (solid lines) derived from data in Fig. 3. The range dependent calibration coefficients in Fig. 2 were used in this analysis. The HSRL measurements are normalized to the molecular backscatter cross section computed from the measured density profile [Fig. 4(a), dashed line] at a height of 1.64 km (ASL). The decrease in the measured HSRL molecular backscatter cross section with increasing range from the aircraft is a direct measure of the attenuation in the atmosphere. The attenuation corrected aerosol backscatter cross section profile [Fig. 4(b), dashed line] shows a clear region above a hazy mixed layer. The error bars represent the maximum variation in the aerosol and molecular backscatter cross sections due to uncertainty in the instrumental calibration.

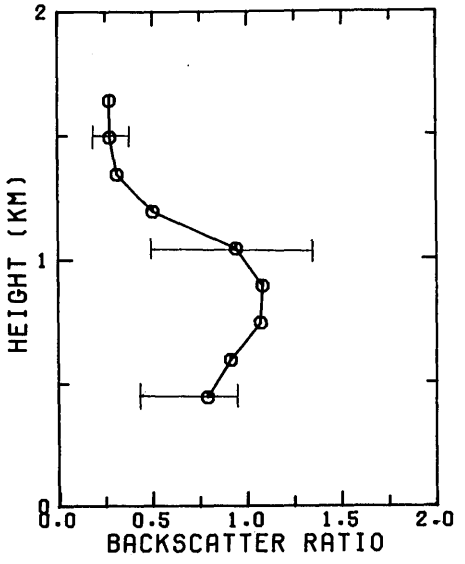

Fig. 5. Aerosol to molecular backscatter ratio S computed from the data using Eq. (6) of Shipley *et al.*[1] The error bars show the maximum variations in S due to calibration uncertainties estimated at the extremes of the 95% confidence level. The calibration errors are largest where the combination of aerosol scattering and uncertainties in the range dependent coefficients have their greatest contributions.

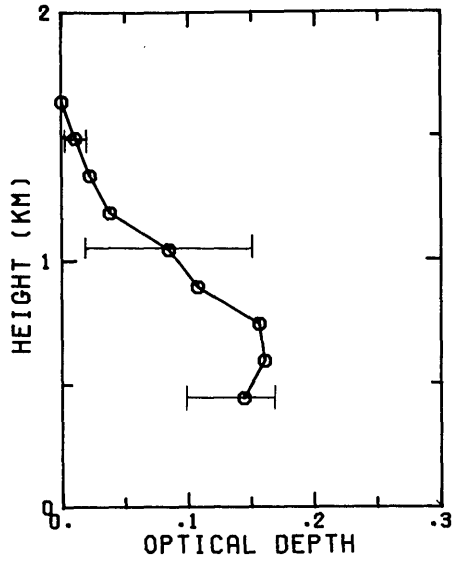

Fig. 6. Optical depth profile $\tau(z)$ using the data shown in Fig. 4(a). The error bars represent the maximum uncertainty due to the calibration procedure described in the text. The apparent negative extinction at the last data point is due to the statistical noise after filtering and averaging.

parameters were obtained from a joint 95% regression confidence region to account for any correlation among the model parameters.[9] The range dependent calibration coefficients were computed for several spectrometer model combinations at the extremes of the 95% confidence level. The ratio of the aerosol coefficients obtained from the surface reflection data was used to constrain further the choice of spectrometer model parameter combinations with the receiver–transmitter geometry. The receiver–transmitter optical axes alignment was adjusted to approximate this surface reflection ratio for each combination of spectrometer model parameters. The error bars shown in Figs. 4–7 represent the maximum uncertainty in the

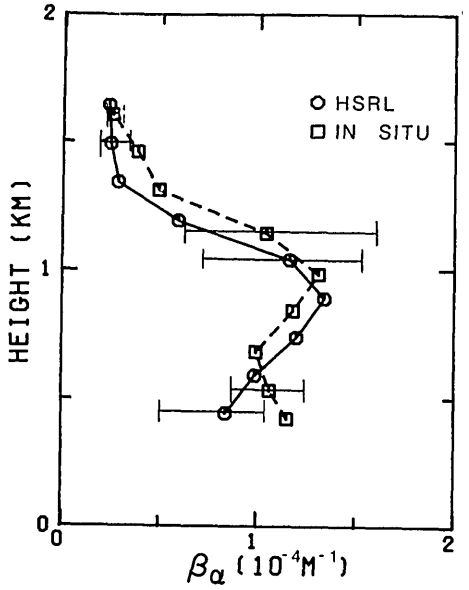

Fig. 7. Intercomparison between HSRL (solid line) and *in situ* nephelometer measurements (dashed line) of the total aerosol scattering cross section derived from the 24 July 1980 data. The *in situ* measurements have been corrected for the desiccation caused by heating the inlet air sample using an optical model described by Sroga.[2] These *in situ* measurements (effective $\lambda = 530$ nm) have been scaled by a $\lambda^{-1.8}$ wavelength dependence for comparison with the HSRL wavelength (467.8 nm). Because of the calibration limitation for this data set, measurements of the backscatter phase function were limited to an average value (0.021 ± 0.003 sr^{-1}) over the data height interval.

HSRL measured optical scattering properties produced by variations in the range dependent calibration.

The signals measured by the dual-channel spectrometer (Fig. 3) are separated into aerosol and molecular components using Eqs. (5a) and (5b) of Shipley *et al.*[1] The separate aerosol and molecular backscatter contributions shown in Fig. 4 have been normalized at 1.64-km ASL to the molecular backscatter cross section computed from an *in situ* temperature profile. The decrease with range in the HSRL measured molecular backscatter from the computed molecular profile is a direct measurement of the optical attenuation in the layer. The aerosol profile corrected for this two-way path attenuation is also shown.

Figures 5 and 6 show the vertical distributions of the aerosol to molecular backscatter ratio S and optical depth τ computed for these data using Eqs. (6) and (8) of Shipley *et al.*[1] The optical depth profile shown in Fig. 6 is calculated as an increasing function of distance from the airborne system. The calibration uncertainty, which depends upon both the magnitude of the aerosol scattering component and the range to the scattering volume, decreases with increasing range and/or decreasing aerosol loading. The calibration uncertainty in these measurements is largest near the top of the mixed layer where the combination of the variations in the calibration range dependence and the aerosol scattering have their maximum contributions.

The aerosol backscatter phase function can be computed from the backscatter ratio and the optical depth assuming that absorption is small compared to the scattering cross section at the HSRL wavelength. The aerosol backscatter phase function $[\overline{IP}_a(\pi)/4\pi]$ averaged over a layer of thickness ΔR is calculated from

$$\frac{\overline{IP}_a(\pi,\overline{R})}{4\pi} = \frac{3}{8\pi} \cdot \frac{\int_R^{R+\Delta R} S(r') \cdot \beta_m(r')dr'}{\omega_0[\Delta\tau(\Delta R) - \Delta\tau_m(\Delta R)]}, \tag{11}$$

where β_m molecular scattering cross section,
ω_0 aerosol single-scatter albedo,
$\overline{R} = R + \Delta R/2$,
$\Delta\tau = \tau(R + \Delta R) - \tau(R)$, and

$$\Delta\tau_m = \int_R^{R+\Delta R} \beta_m(r')dr'.$$

The backscatter phase function for these data can only be measured with sufficient accuracy over an optically thick layer due to calibration and statistical uncertainties. A more thorough presentation of the calibration uncertainties is given elsewhere.[2] The aerosol backscatter phase function averaged over the entire depth of the data (~1.6 km) was measured to be 0.021 sr^{-1} with an uncertainty due to calibration procedure of 0.003 sr^{-1}. This value is consistent with Mie calculations for aerosol models[10,11] and measurements by other investigators.[12]

The HSRL derived aerosol scattering cross-section measurements [Eq. (11) of Ref. 1] obtained during the flight evaluation experiment were compared with the *in situ* measurements obtained by a heated integrating nephelometer located on board the instrumented light aircraft.[8] Because of changes in aerosol particle size and composition due to heating of the inlet air, the optical properties measured inside the nephelometer can be different from those in the atmosphere. An optical model has been applied to calculate the effects of particle swelling on aerosol optical properties.[2] Mie scattering theory is used in conjunction with the particle growth given by Nilsson[13] to compute changes in aerosol scattering properties with relative humidity. The *in situ* humidity measurements along with this optical model have been used to correct the nephelometer measurements for the heated inlet desiccation effects. The nephelometer measurements (center wavelength ~530 nm) have been scaled by a wavelength dependence $[\beta_a(\lambda)\alpha\lambda^{-1.8}]$ for intercomparison at the HSRL wavelength (467.8 nm).[14]

The comparison between the corrected nephelometer and HSRL measurements of the aerosol scattering cross section is shown in Fig. 7. Because of the calibration limitation in backscatter phase function measurements for this data set, the backscatter phase function altitude profile was not derived from HSRL data. Because the backscatter phase function can also vary with humidity, the same optical model used to correct the nephelometer measurements has been applied to the HSRL profile. The *in situ* humidity profile is used for this correction. The error bars on the HSRL measurements of the aerosol scattering cross section represent the maximum uncertainty due to calibration errors and backscatter phase function variations associated with uncertainties

in the measured humidity. The error bars on the *in situ* measurements show the one standard deviation variation in the individual measurements combined with the humidity uncertainties of the optical model correction.

V. Conclusions

This paper has described the instrumental calibration and data analysis procedures for the high spectral resolution lidar system. The range dependence of the instrument calibration is based upon modeling the receiver spectral bandpass distribution of the dual-channel spectrometer and the angular distribution of backscattered light. An error analysis for the derived optical properties is discussed for instrumental uncertainties in the tuning, calibration, and optical alignment of the HSRL system.

The experimental results obtained on 24 July 1980 demonstrate the unique ability of the HSRL to measure remotely optical scattering properties of atmospheric aerosols from an airborne platform. The combined use of high spectral resolution, a narrow receiver field of view, and low pulse energies allows eyesafe daytime operations of the HSRL. The vertical distribution of the HSRL measured aerosol scattering cross section shows favorable agreement with *in situ* integrating nephelometer measurements.

An error analysis of the HSRL data has pointed to directions for improvements in the HSRL system. The receiver–transmitter configuration has been changed to a coaxial arrangement to minimize the range dependence of the calibration coefficients. A $CuCl_2$ vapor laser transmitter has been incorporated to increase the transmitted power and improve photon counting statistics. The extreme sensitivity of the HSRL calibration and wavelength stability to environmental temperature has been traced to defective etalon holders, and these have been replaced. The improved system is being prepared for ground based testing. The instantaneous profile capabilities of the HSRL combined with the mobility of the airborne platform provide a unique tool for measuring the spatial distribution of atmospheric aerosols on a regional scale.

We wish to thank James A. Weinman of the Department of Meteorology, University of Wisconsin, Madison, for his comments during preparation of this paper.

The efforts of the technical staff at the NASA Wallops Flight Center during the installation and testing of the HSRL system on board the Wallops Electra are greatly appreciated.

This research was supported under NASA contracts NASA-14136 and NAG-1-212. We thank Edward V. Browell of the NASA Langley Research Center for his contributions as contract monitor.

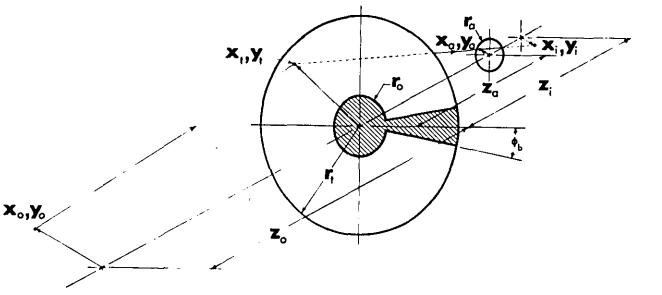

Fig. 8. Schematic of the geometry used for computing the aperture intensity distribution with a lens of focal length f centered in the x-y plane at $z = 0$, a secondary obstruction ($r = r_s$), and a transmitter baffle (half angle = ϕ_a). The telescope aperture ($r = r_a$) is located at a position $z = z_a$ to allow adjustments of the telescope focus. The ray from the object point (x_o,y_o,z_o), which passes through the image point (x_i,y_i,z_i) and a point x,y in the aperture plane ($z = z_a$), has an intercept in the lens plane ($z = 0$) of x_t,y_t. If the point x_t,y_t falls inside the usable portion of the telescope, that ray contributes to the aperture intensity distribution.

Appendix. Estimation of the Range Dependence of the Aperture Intensity Probability Distribution

In this Appendix we describe the calculation of the intensity distribution of backscattered light in the spectrometer entrance aperture. The receiver telescope is modeled as a simple lens with obstructions for the secondary mirror and laser baffles. The energy distribution in the transmitter beam pattern is assumed to be Gaussian. Figure 8 illustrates schematically the geometry of the model. A simple ray tracing technique is used to determine if a ray originating from a point (x_o,y_o,z_o) in the object space ($z_o > f$) and passing through a point (x,y) in the aperture plane ($z = z_a$) intercepts a usable portion of the telescope lens plane. The lens plane intercept point (x_t,y_t) is calculated from the geometry in Fig. 8:

$$x_t = x_i + \frac{(x - x_i)}{(1 - z_a/z_i)}; \qquad y_t = y_i + \frac{(y - y_i)}{(1 - z_a/z_i)}. \tag{A1}$$

The coordinates of the image (x_i,y_i,z_i) of an object point (x_o,y_o,z_o) are given by the lens equation

$$x_i = -x_o f_t/(z_o - f_t); \; y_i = -y_o f_t/(z_o - f_t); \quad z_i = -z_o f_t/(z_o - f_t), \tag{A2}$$

where f_t is the focal length of the telescope lens.

The fraction of the total received light intercepted by an area $dxdy$ centered at x,y in the aperture can be estimated by

$$I_a[x,y,z_a,\zeta(x_o,y_o,R)]dxdy = \int_{-\infty}^{\infty}\int_{-\infty}^{\infty}\left[\zeta(x_o,y_o,R)\frac{dxdy}{\pi r_e^2}\right]dx_o dy_o \tag{A3}$$

for $r_o^2 \le (x_t^2 + y_t^2) \le r_t^2$

$|\tan^{-1}(y_t/x_t)| > \phi_b$

$= 0$ otherwise,

where $I_a(x,y,z_a,\zeta)dxdy$ fraction of received light intercepted by an area $dxdy$,

$\zeta(x_o,y_o,R)$ normalized Gaussian beam pattern so that integration of ζ in the plane perpendicular to the z axis is equal to unity,

r_t radius of receiver telescope,

r_o radius of secondary obstruction,

r_e radius of illuminated spot in the aperture plane,

$r_e = r_t(1 - \{[|z_a|(|z_a| - f)]/(z_o \cdot f)\})$, and

ϕ_b half angle of sector obstructed by laser beam baffle in telescope.

The aperture intensity distribution is numerically computed for a given range R at a discrete number of data points in the spectrometer aperture using Eqs. (A1)–(A3).

References

1. S. T. Shipley, D. H. Tracy, E. W. Eloranta, J. T. Trauger, J. T. Sroga, F. L. Roesler, and J. A. Weinman, Appl. Opt. **22**, same issue (1983).
2. J. T. Sroga, "Remote Measurements of Tropospheric Aerosol Scattering Properties by an Airborne High Spectral Resolution Lidar," Ph.D. Thesis, U. Wisconsin (1983).
3. G. Fiocco and J. B. DeWolf, J. Atmos. Sci. **25**, 488 (1968).
4. S. Yip, J. Acoust. Soc. **49**, 941 (1971).
5. S. Yip and M. Nelkin, Phys. Rev. A **135**, 1241 (1964).
6. J. E. Mack, D. P. McNutt, F. L. Roesler, and R. Chabbal, Appl. Opt. **2**, 873 (1963).
7. D. W. Marquardt, J. Soc. Ind. Appl. Math. **11**, 431 (1963).
8. G. L. Gregory, S. M. Beck, and J. J. Mathis, Jr., NASA Tech. Memo. 83107 (1981).
9. N. R. Draper and H. Smith, *Applied Regression Analysis* (Wiley, New York, 1981).
10. E. P. Shettle and R. W. Fenn, AFGL-TR-79-0214, No. 676 (1979).
11. D. Deirmendjian, *Electromagnetic Scattering on Spherical Polydispersions* (American Elsevier, New York, 1969).
12. J. D. Spinhirne, J. A. Reagan, and B. M. Herman, J. Appl. Meterorol. **19**, 426 (1980).
13. B. Nilsson, Appl. Opt. **18**, 3457 (1979).
14. N. C. Ahlquist and R. J. Charlson, Atmos. Environ. **3**, 551 (1969).

Meetings Calendar

December

? 12th Int. Laser Radar Conf., Melbourne *C. Platt, CSIRO, Div. of Atmospheric Physics, P.O. Box 77, Mordiattoc, Victoria 3195, Australia*

5–6 Int. Electron Devices Mtg., Wash., D.C. *M. Widerkehr, Courtesy Assoc., 1629 K St., N.W., Wash., D.C. 20006*

5–9 Fundamentals of Conventional & Laser Spectroscopy course, Orlando *Ed Dir., Laser Inst. of Amer., 5151 Monroe St., Ste. 118W, Toledo, Ohio 43623*

6–8 Advanced Geological Remote Sensing course, Wash., D.C. *Cont. Eng. Ed., George Wash. U., Wash., D.C. 20052*

12–16 6th Int. Conf. on Lasers & Applications, San Francisco *SOQE, P.O. Box 245, McLean, Va. 22101*

12–17 8th Ann. Int. Conf. on Infrared & Millimeter Waves, Miami Beach *K. Button, MIT Nat. Magnet Lab., Bldg. N.W. 14, Cambridge, Mass. 02139*

12–25 Holography & Speckle Winter School, Bangalore *S. Ramprasad, Winter School on Holography & Speckle, Central Instruments & Services Lab., Indian Inst. of Science, Bangalore-560 012, India*

1984

January

9–11 Experimental Mechanics of Fiber Reinforced Composite Materials seminar, San Diego *SESA, 14 Fairfield Dr., Brookfield Ctr., Conn. 06805*

9–20 Optical Science & Eng. course, Tucson *P. Slater, P.O. Box 18667, Tucson, Ariz. 85731*

16–20 Laser Beam Propagation & Interaction Effects course, Huntsville *Eng. Tech., Inc., P.O. Box 8859, Waco, Tex. 76714*

22–27 SPIE Technical Symp., Los Angeles *SPIE, P.O. Box 10, Bellingham, Wash. 98227*

23–25 **Optical Fiber Communication, OSA/IEEE Top. Mtg.,** New Orleans *OSA, Mtgs. Dept., 1816 Jefferson Pl., N.W., Wash., D.C. 20036*

25–27 31st Ann. Western Spectroscopy Assoc. Conf., Pacific Grove *D. Saperstein, IBM Instruments, 40 W. Brokaw Rd., San Jose, Calif. 95110*

February

12–15 Color & Imaging Conf., Williamsburg *F. Billmeyer, Jr., Chem. Dept., Rensselaer Poly. Inst., Troy, N.Y. 12181*

13–17 Laser Fundamentals & Systems course, Dallas *Eng. Tech., Inc., P.O. Box 8859, Waco, Tex. 76714*

continued on page 3777